Thermal cracking of n -butylbenzene at high pressure: Experimental study and kinetic modelling

N.C. C Leguizamon Guerra, J.C. C Lizardo Huerta, C. Lorgeoux, R. Michels, R. Fournet, B. Sirjean, A. Randi, R. Bounaceur, V. Burklé-Vitzthum

THERMAL CRACKING OF N-BUTYLBENZENE AT HIGH PRESSURE: EXPERIMENTAL STUDY AND KINETIC MODELLING

N. C. Leguizamon Guerra [a,b], J. C. Lizardo Huerta[a], C. Lorgeoux[b], R. Michels[b], R. Fournet[a], B. Sirjean[a], A. Randi[b], R. Bounaceur[a],V. Burklé-Vitzthum[a*]

[a] Laboratory of Reactions and Process Engineering, LRGP UMR 7274, CNRS, Université de Lorraine BP 20451, 54001 Nancy, France

[b] GeoRessources UMR 7359, CNRS, Université de Lorraine BP 70239, 54501 Vandœuvre-lès-Nancy, France

* Corresponding author. Tel.: +33372743816

E-mail address: valerie.vitzthum@univ-lorraine.fr (V. Burklé-Vitzthum).

Keywords: pyrolysis, detailed kinetic modelling, alkylbenzene, high pressure, free-radical reactions

Highlights

- Pyrolysis of *n*-butylbenzene at 70 MPa and from 583 K to 623 K was performed in sealed gold tubes.
- The main products are toluene, ethylbenzene, iso-heptyl- and iso-butylbenzene, CH_4 and C_2H_6.
- A detailed kinetic model was constructed and validated over the entire experimental range of conversion (0.7-62%).
- Thermochemical and kinetic parameters of key decomposition routes were computed using theoretical calculations.

Graphical abstract

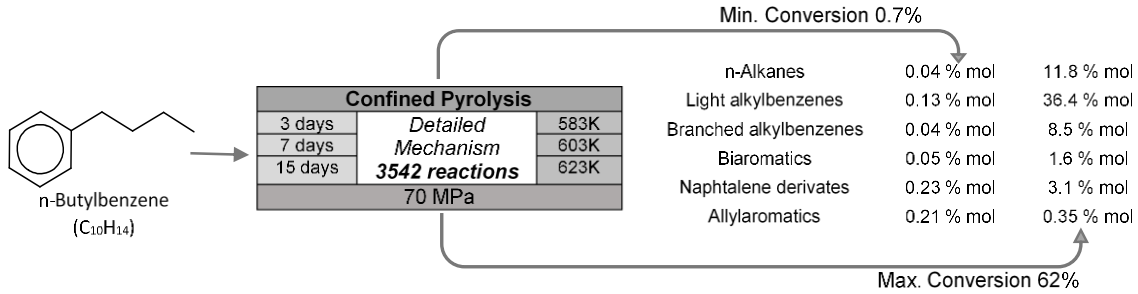

Abstract

The thermal cracking of *n*-butylbenzene was experimentally studied at high pressure (70 MPa), and moderate temperatures (583, 603, 623 K), for conversions of *n*-butylbenzene ranging between 0.7% and 62%. The pyrolysis was performed in sealed isobaric gold tubes (confined pyrolysis). Three main chemical families were observed: short alkylbenzenes (mostly toluene and ethylbenzene), branched alkylbenzenes (isomers of iso-butylbenzene and iso-heptylbenzene) and short alkanes (from CH_4 to C_4H_{10}). As minor products, alkenylbenzenes (styrene and butenylbenzene), methylindane and biaromatic structures were also quantified.

A detailed kinetic model composed of 3542 free-radical reactions and 383 species (molecules and free-radicals) was written in a systematic manner by taking into account all relevant elementary free-radical reactions. A large number of thermochemical and kinetic parameters were computed by theoretical calculations. A very good agreement between experimental and simulation results is observed for every operating condition and for most major and minor compounds.

The apparent kinetic parameters were computed at 623 K, 70 MPa and 30% conversion under the assumption of a first-order global rate law: the apparent activation energy was found equal to 66.6 kcal/mol and the frequency factor to 6.3×10^{16} s^{-1}. The extrapolation to low temperature (473 K), which is characteristic of deeply buried oil reservoirs, shows that the stability of *n*-butylbenzene is about the same as the stability of alkanes, but *n*-butylbenzene is more stable than *n*-decylbenzene and less stable than toluene.

1. Introduction

In order to assess the thermal evolution of oils in reservoirs during geological time (up to million years), it is mandatory to set up robust kinetic models ([1], [2] and [3]) for the thermal reactions occurring at high pressure (10-100 MPa) and low temperature (423-493 K). Consequently, it is necessary to simulate the thermal reactions at the laboratory scale by conducting pyrolysis of oils (e.g. [4], [5], [6] and [7]), oil fractions (e.g. [5]) or model compounds (e.g. [8]) at pressures as high as in geological reservoirs, but at higher temperatures (623-773 K), in order to compensate for the geological time and to be able to decrease the reaction time (a few hours to several weeks in the laboratory). Modelling oil fractions by pure hydrocarbons or simple mixtures allows the construction of detailed kinetic models for thermal cracking (e.g. [9] and [10]), based on elementary steps (mainly free-radical reactions) with their fundamental kinetic parameters. The main advantage of these models is their precision as well as the possibility of extrapolation to geological temperatures since the main reaction pathways and the fundamental kinetic parameters remain unchanged over a temperature range of 200 K.

The aromatic fraction represents up to 40% (mass) of conventional oils and the polar compounds (NSO compounds), which represent up to 20% (mass) of conventional oils, also contain numerous aromatic structures ([3] and [11]). That is why several experimental studies of thermal cracking of alkylbenzene can be found in the literature: alkylbenzenes are taken as model compounds of the aromatic fraction ([12], [13] and [14]) or as model compounds of asphaltenes [15] or even of heavy oils [16]. A few studies include detailed kinetic modelling at high pressure ([17], [18], [19], [20], [21] and [22]) or in supercritical water conditions [22]. In those studies, pressure is usually in the range of 0.2-14 MPa and temperature is usually greater than 673 K, except for the studies [18] and [20] conducted at 70 MPa and temperatures lower than 623 K. Main products of the pyrolysis of alkylbenzenes (C_nH_{2n+1}-C_6H_5) are usually grouped into two pairs: toluene and $C_{n-1}H_{2n}$/$C_{n-1}H_{2n-2}$ as well as ethylbenzene and/or styrene and $C_{n-2}H_{2n-2}$ ([14] and [15]).

This paper aims to construct and validate a detailed and robust kinetic model for the thermal cracking of *n*-butylbenzene. Shorter alkylbenzenes like toluene [20] and longer alkylbenzenes like *n*-decylbenzene [18] were already exhaustively studied, contrary to *n*-butylbenzene [14]. For this

purpose, new experimental data has been obtained from confined pyrolysis experiments (sealed gold cells [23], [24] and [25]), for a pressure characteristic of deep reservoirs (70 MPa) and for large temperature (583-623 K) and conversion (0.7–62 %) ranges. On the other hand, a kinetic model has been written in a comprehensive way for the primary consumption of *n*-butylbenzene and the main products. Most of the thermochemical and kinetic parameters of the *n*-butylbenzene main decomposition routes were computed by electronic structure calculations to improve the reliability of the model. Finally, the reactivity of *n*-butylbenzene at geological pressure and temperature conditions was compared with other common hydrocarbons.

2. Experimental and analytical procedure

n-butylbenzene (purity ≥ 99+%), was obtained from Sigma Aldrich and used as received.

2.1. Loading procedure and pyrolysis device

Confined pyrolysis was carried out in gold cells (purity 99.99%, 5 cm length, 5 mm i.d. and 0.5 mm wall thickness) sealed at one end and loaded with 100 µL of *n*-butylbenzene. The details of the confined pyrolysis were given elsewhere ([23] and [24]). Monthioux et al. [25] showed that the reactor configuration and the experimental conditions lead to results compatible with the thermal evolution of hydrocarbons in the geological petroleum reservoirs.

The gold tubes were sealed by pulse arc-welding in a bath of liquid nitrogen, and then placed in a pressurized autoclave. The pressure was set to 70 MPa and the temperatures to 583, 603 and 623 K (± 1 K). The pyrolysis duration was 3 days, 7 days and 15 days. At the end of the pyrolysis, the autoclaves were rapidly cooled to room temperature in a water heat exchanger. For each condition, four replicates were performed for the quantitation of the gaseous and liquid products. The pyrolysis of a supplementary gold cell was performed at 623 K for 15 days and used for identification of the liquid products.

2.2. Analytical procedure

For the identification of the liquid products, the gold cell was opened at both ends in a vial containing dichloromethane. Extraction was performed in an ultrasonic bath during 1 hour. The compounds were identified by GC-MS (Shimadzu GCMS-QP 2010 Plus; carrier gas: He) using a Zebron ZB 5-MS column (Phenomenex, length: 60 m, 0.25 mm i.d., 0.10µm film, 5%-Phenyl, 95%-dimethylpolysiloxane phase). The temperature program was set as following: the initial temperature was set at 313 K during 3.5 min, then a heating rate of 6 K/min was applied up to 593 K, and the final temperature was kept during 10 min.

The quantification of all gaseous and liquid products was performed by a Thermodesorption-GC-FID (Shimadzu GC2010 Plus; carrier gas: H_2) using a Zebron ZB 5-MS column (Phenomenex, length: 60 m, 0.25 mm i.d., 0.10 µm film). A GC-FID is connected to an oven (Top Industrie conception) in which the gold cells are pierced and the products are thermally desorbed (Fig. 1). The GC is equipped with a cryogenic focus temperature controller, which allows freezing the top of the column at 78 K during 2 minutes using liquid nitrogen. This methodology separates methane and improves the separation of condensable gases (C_2 to C_4). It allows the analysis of gaseous and liquid products during the same analysis and normally avoids co-elution of the gases. Nevertheless, no propylene was detected, although it was *a priori* expected ([14], [15] and [18]), since it was described as the co-product of toluene in previous studies. It can be assumed that it could be co-eluted with other gases, although gas peaks are well defined and show no shoulders that could suggest co-elutions. This will be discussed later. The temperature program was set as following: the initial temperature was set to 303 K during 4 min, then a heating rate of 6 K/min was applied up to 593 K, and the final temperature was kept during 10 min. The calibration of the FID was done by a gas mixture obtained from Air Liquide (Ar: 14.9600%; CO_2: 24.9800%; CH_4: 30.0300%; C_2H_6: 13.0400%; C_3H_8: 8.9660%; C_4H_{10}: 7.0240%; C_5H_{12}: 1.0022%) and by using commercially available standard compounds for the liquids. For each quantified compound, an external calibration curve was drawn with 6 concentrations by using a basis of 100µL of *n*-butylbenzene (nBB). Light hydrocarbons from the Air Liquid gas mixture were calibrated from 0.28 µmole/100µL nBB to 59.89 µmole/100µL nBB. Calibration range for heavier compounds varied from 0.05 µmole/100µL nBB to 14.20 µmole/100µL nBB. During a sequence, calibration controls were injected to check the overall calibration.

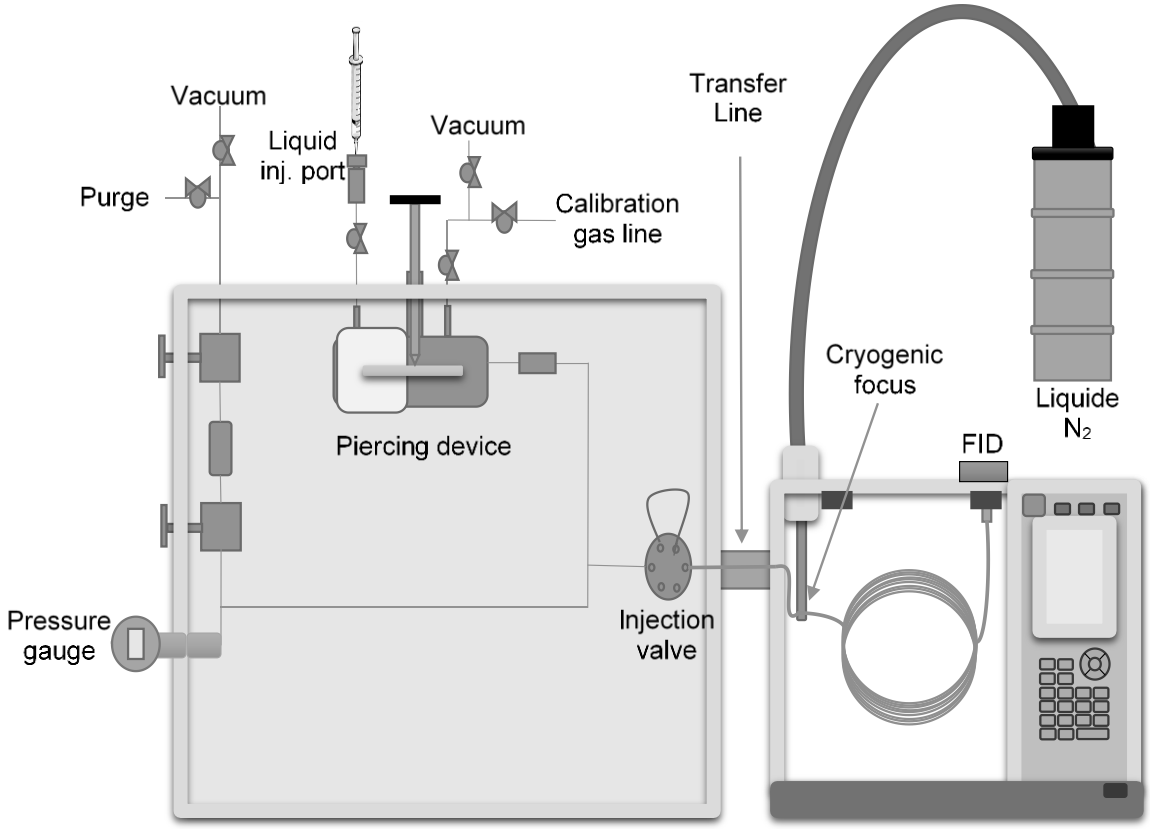

Figure 1. Schematic diagram of the oven containing the piercing device for the gold cells and the GC-FID.

The remaining quantity of *n*-butylbenzene was too high to be determined directly by Thermodesorption-GC-FID (saturation of the detector). In order to quantify *n*-butylbenzene, a gold cell was cut, extracted and diluted before analysis by GC-FID (Agilent Technologies 7890 A). 1 µL of the sample was directly injected in splitless mode in the GC by a syringe. This GC-FID used the same column, the same carrier gas and almost the same temperature program (final temperature kept for 20 min instead of 10 min) as the Thermodesorption-GC-FID. Quantification was carried out using

internal calibration. An internal standard (*n*-C_{20}) has been added after opening of the gold cell for the quantification. *n*-C_{20} has been chosen for this study because it is not a reaction product and it does not co-elute with any product. For each quantified compound, a calibration curve was derived from 7 concentrations (from 1.19×10^{-5} µmole/µL to 2.11×10^{-4}, µmole/µL). During a sequence, calibration controls were injected every 10 samples to check the overall calibration.

The error-bars presented in the figures correspond to the standard deviation of the four replicates. The standard deviation is about 10% or less, except at low conversion (20-50 %), which is due to the lack of precision of the measurements at very low concentration. Moreover, a high standard deviation is observed for the gas at 623 K – 15 days (and not for the heavier compounds), for which we have no explanation.

3. Experimental results

The conversion of *n*-butylbenzene was calculated by the sum of the ratio X_i of the products, which is defined by *eq. 1*:

$$X_i = \frac{n_{compound\ i}}{n^0_{BB}} \qquad eq.1$$

Where $n_{compound\ i}$ is the amount (in moles) of the compound i and $n°_{BB}$ the initial amount (in moles) of *n*-butylbenzene. This ratio is very close to the molar fraction x_i if the molar expansion is negligible, which is the case at low and moderate conversion for the pyrolysis of pure hydrocarbons.

The quantification of the remaining *n*-butylbenzene was not precise enough to allow calculation of the conversion, especially at low values. That is why the conversion was determined on the basis of the products.

The experimental conditions lead to conversions from 0.7% (583K - 3 days) to 62% (623K – 15 days) (Table 1).

At low conversion (0.7%), the main products are styrene, methylindane, indane, butenylbenzene (sum of the isomers), toluene and iso-heptylbenzene (sum of the isomers), in decreasing order of importance.

At high conversion (62%), the main product becomes toluene, which is 5 times more abundant than the second main product that is iso-heptylbenzene (the sum of the different isomers). The other major products are iso-butylbenzene (1-methylpropyl- and 2-methylpropylbenzene), methane, ethylbenzene, ethane and methylindane, in decreasing order of importance. A typical GC chromatogram obtained for the products at high conversion is presented in Fig.2.

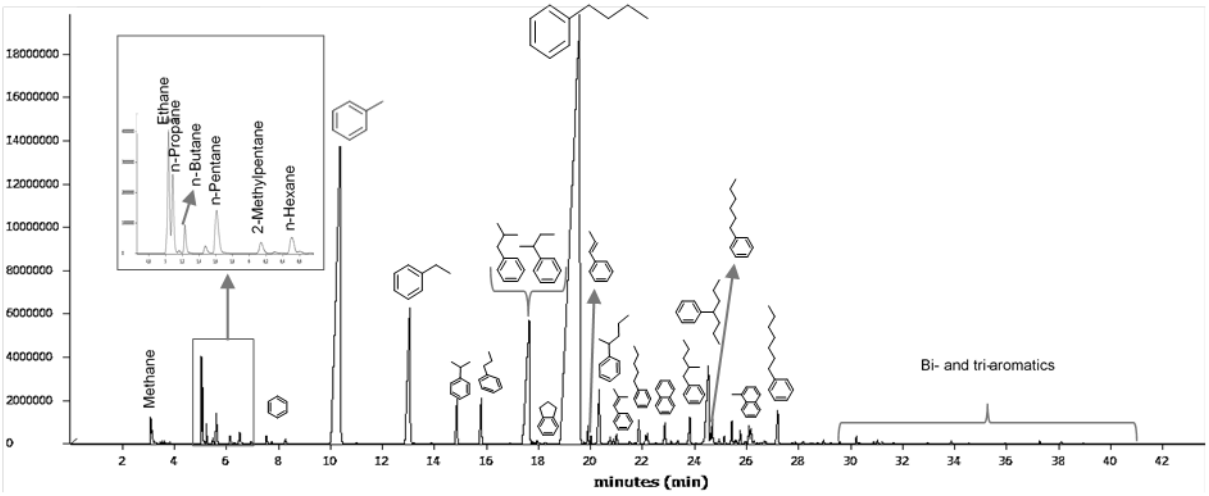

Figure 2. Example of GC-FID-chromatogram obtained after pyrolysis of *n*-butylbenzene at 623K, 70 MPa, during 15 days (62% conversion).

A great number of less abundant products were also identified and quantified: other light alkanes from C_3 to C_7, benzene, styrene, *n*-propylbenzene and iso-propylbenzene, branched alkylbenzenes (alkyl chain from C_5 to C_{10}), butenylbenzene, benzene, tetralin, methylnaphthalene and biaromatic compounds (e.g. bibenzyl). The yield and selectivity of the main products are given in Supplementary Material 1.

In the literature ([14], [15], [18] and [22]), toluene is always described as the main pyrolysis product of alkybenzenes. Toluene is usually accompanied by an alkene and an alkane $C_{n-1}H_{2n}/C_{n-1}H_{2n-2}$ ([14], [15] and [18]) which would be propane and propylene in the case of *n*-butylbenzene. In our experiments, propane has been detected as a minor product, but propylene was not observed. It should be noted that in the case of *n*-hexylbenzene, pentane and pentene ($C_{n-1}H_{2n}/C_{n-1}H_{2n-2}$ in the case of *n*-

hexylbenzene) are described in the literature [22], but as minor products because consumed by secondary reactions. This is overall in agreement with our results.

In the literature, formation of styrene is described at low pressure [15] or both styrene and ethylbenzene at intermediate pressure [22]. At high pressure [18], ethylbenzene is one of the major reaction products and styrene a minor product as it is observed in our experiments. $C_{n-2}H_{2n-2}$, which is ethane in our study, is an important reaction product as underlined in the literature ([14], [15], [18] and [22]).

The mass balance *M.B* has been calculated according to *eq. 2*:

$$M.B = \frac{\sum_i M_i \times X_i}{M_{BB}} \times 100 \qquad \textit{eq. 2}$$

Where M_i is the molecular mass of the compound i, M_{BB} the molecular mass of *n*-butylbenzene and X_i the ratio defined by *eq1*.

The mass balance (Table 1) is between 85% and 94% and the mean value is 91%. These results are globally satisfying.

Table 1. Conversion and mass balance of pyrolysis of *n*-butylbenzene.

Temperature (K)	Time (days)	Conversion (%)	Mass balance (%)
583	**3**	0.7±0.1	91±1
	7	1.5±0.4	90±1
	15	2.0±0.2	85±1
603	**3**	2.2±0.2	90±1
	7	7.8±1.2	94±2
	15	10.4±1.2	90±1
623	**3**	13.5±0.2	92±3
	7	32.7±0.7	93±2
	15	62.1±6.2	91±3

4. Kinetic modelling of the thermal cracking of *n*-butylbenzene

The kinetic model is composed of 3542 free-radical reactions with their kinetic parameters, and 383 species (molecules and free-radicals) with their thermochemical parameters in the NASA polynomial format. The kinetic model has been written in a systematic manner by taking into account all relevant elementary free-radical reactions: unimolecular initiations, bimolecular initiations, ipso-additions, H-transfers, isomerizations (monomolecular and bimolecular), decompositions by β-scissions, additions of radicals to double bonds, terminations by recombination and disproportionation, as well as some pericyclic reactions which are also elementary molecular reactions. The kinetic model in the CHEMKIN II format [26] is given in Supplementary Material 2, as well as the nomenclature of the species (Supplementary Material 3). The kinetic parameters were not tuned to improve agreement between experiments and simulations.

Most of the reactions were written as reverse, and thus were automatically taken into account in the kinetic model. The corresponding kinetic parameters are computed by using the kinetic parameters of the direct reaction and the thermochemical parameters. So the precision of the thermochemical parameters is of utmost importance.

4.1. Theoretical calculation of the rate coefficients

Important reactions involved in the pyrolysis of *n*-butylbenzene have been studied by means of electronic structure calculations and rate coefficients have been calculated from computed potential energy surfaces (PES). The CBS-QB3 [27] method, implemented in Gaussian 09 [28], was used to compute the energies at 0K of minima and saddle points of the PES. This composite method includes geometry optimization and frequency calculations at the B3LYP/CBSB7 level of theory. CBS-QB3 is an efficient method which allows a good compromise between accuracy and computation time, for large molecules such as *n*-butylbenzene. Canonical Transition State Theory (TST) has been applied to deduce rate constants from energy and frequency calculations. In the case of unimolecular reactions involving a barrier height $V^{\neq}$ at 0 K, the rate constant can be computed from *eq. 3*:

$$k(T) = \kappa L \frac{k_B T}{h} \frac{Q_{TS}(T)}{Q_R(T)} exp\left[-\frac{V^{\neq}}{RT}\right] \qquad eq.3$$

In order to obtain the accurate partition function Q_i (Q_{TS} and Q_R) to reach a sufficient precision in computed *k(T)* and thermochemical data (entropy and heat capacity of the species), all internal rotations between C-C bonds have been considered as hindered rotors (HR) rather than harmonic oscillators (HO). Internal rotors treatment included relaxed scans performed at the B3LYP/cbsb7 level of theory for each rotor *j*, with Gaussian 09. The resulting torsional potential curves were fitted with Fourier series (10 cosines and 10 sines) and used to solve the one-dimensional Schrodinger equation (1DHR method [29]), which allows the calculation of the HR partition function $q_{1-DHR,j}$. In addition, the torsional potential was used to recalculate the harmonic partition function ($q_{HO,j}$) corresponding to the rotor *j*, but treated as a one-dimensional uncoupled mode [30]. Finally, the partition function *Q* can be expressed as:

$$Q = Q_{HO} \prod_{j=1}^{N} \frac{q_{1-DHR,j}}{q_{HO,j}} \qquad eq.4$$

where *N* is the total number of hindered rotors, and Q_{HO} is the global partition function in the harmonic oscillator approximation and obtained from Gaussian 09.

Moreover, for reactions involving a H-atom transfer, the rate constant was multiplied by a transmission coefficient, κ (*eq. 3*). This parameter was obtained using the one dimensional asymmetric Eckart potential method to take into account tunneling effect [31]. Due to the low temperatures considered in this study, this parameter can play a significant role on the value of the rate constant (factor 2 to 3). In addition, the rate constants is weighted by a statistical factor L (*eq. 3*) which takes into account the number of optical isomers and external symmetries in the TS and in the reactant, according to *eq. 5*:

$$L = \frac{\sigma_R \times n_{TS}}{\sigma_{TS} \times n_R} \qquad eq.5$$

where σ_R and σ_{TS} are the external symmetry of, respectively, the reactant and the transition state, while n_R and n_{TS} correspond to their number of optical isomers. Note that using *eq. 5* in *eq. 3* required removing the external symmetry numbers of the external rotational partition functions in *Q*.

Finally, the rate constants computed at several temperatures allows deducing the rate coefficients expressed as a modified Arrhenius law (*eq. 6*):

$$k = A\ T^n \exp\frac{-E}{RT} \qquad eq.6$$

where A is the pre-exponential factor (mol, cm^3, s^{-1}); n the temperature exponent and E is the activation energy (cal mol^{-1}).

All of the thermokinetic parameters have been calculated using the THERMROT software [32]. The geometries of the Transition States are given in Supplementary Material 4.

4.2. Development of the kinetic model

4.2.1. Detailed description of the primary mechanism

The kinetic model of the thermal cracking of *n*-butylbenzene is composed of several sub-mechanisms. The first is a detailed primary mechanism of *n*-butylbenzene. The primary mechanism only involves *n*-butylbenzene and the subsequent radicals formed as reactants. This part of the mechanism is comprehensive and contains all possible elementary reactions described below. On the other hand, the molecules formed in the primary mechanism react in a secondary mechanism. Due to the large number of primary molecules generated, only the most important products have been considered in this part of the mechanism. To this end, simulations have been carried out by considering only the primary mechanism. Through this approach, it was possible to select major primary molecules and radicals and to develop the secondary mechanism by considering all possible elementary reactions between these species. The same procedure was used to select the major products to consider in the tertiary mechanism. In this case the simulations were performed by considering only the primary and secondary mechanisms. Finally, this approach was repeated until the entire mechanism contains the important products observed experimentally. The last part of the mechanism is composed of a C_0-C_2 reaction database [33] and contains all the elementary reactions involving species having less than three carbon atoms. To generate this mechanism, the following elementary reactions have been considered: unimolecular initiations, bimolecular initiations, ipso-additions, H-transfers, isomerizations, decomposition by β-scission, ring-closure reactions, pericyclic reactions, and terminations.

In the case of *n*-butylbenzene, the Bond Dissociation Energies (BDE) were first computed [28] at the CBS-QB3 level of theory. As expected [18], the weakest BDE are related to the C-C and the C-H bonds in β-position of the aromatic cycle (Fig.3). However, all the unimolecular initiations involving the dissociation of the C-C and C-H bonds of the alkyl chain were taken into account in the mechanism. For these reactions, activation energies have been taken equal to BDE, while the *A* factor has been obtained from thermokinetic relationships, based on the fact that the reverse reactions (combinations) are barrierless.

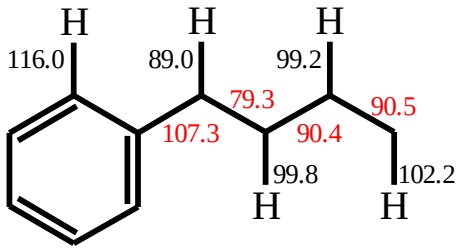

Figure 3. Bond Dissociation Energies of *n*-butylbenzene at 298 K (kcal.mol^{-1}).

The bimolecular initiations correspond to the reverse of the termination reactions by disproportionation. The bimolecular initiations between two *n*-butylbenzene molecules which imply a loss of aromaticity, were considered (Fig. 4), because a previous study on the pyrolysis of toluene highlighted their importance [20]. Therefore, the kinetic parameters *A* and *n* were taken from [20], and the activation energy, which corresponds to the enthalpy of reaction in this case, was calculated by theoretical calculations at the CBS-QB3 level of theory. This approach ensures consistency between kinetic and thermochemical data.

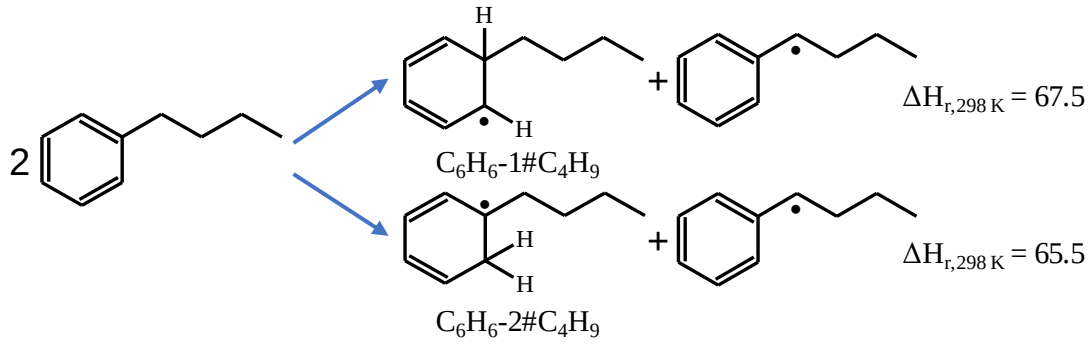

Figure 4. Bimolecular initiations between two molecules of *n*-butylbenzene (CBS-QB3 enthalpies of reaction at 298 K, in kcal.mol^{-1}).

Ipso-additions (Fig. 5) of the H$^{\cdot}$, methyl, ethyl, propyl, iso-propyl and propen-3-yl ($C_3H_5^{\cdot}$) radicals to *n*-butylbenzene were considered. The kinetic parameters of the ipso-additions of the H$^{\cdot}$ radical were taken by analogy from Baulch et al. [34]. Two reaction rate rules were determined using theoretical methods. The high-pressure limit rate constants of the ipso-additions of CH_3 and C_3H_5 on ethylbenzene were calculated at the CBS-QB3 level of theory. Ethylbenzene was used to limit the size of the molecular system while maintaining the accuracy of computed kinetic parameters. The calculated rate coefficients (Table 2) were used in the following rate rules: the kinetic parameters of ethylbenzene + CH_3 were used for the ipso-addition of alkyl radicals on *n*-butylbenzene and the rate constant of ethylbenzene + C_3H_5 was used for the additions of resonance stabilized radicals.

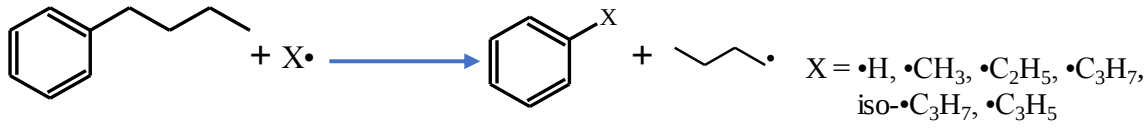

Figure 5. Ipso-addition of radicals to *n*-butylbenzene.

Table 2. Kinetic parameters of the ipso-additions computed by theoretical calculations at the CBS-QB3 level of theory.

Ipso-addition	A ($cm^3.mol^{-1}.s^{-1}$)	n	E ($cal.mol^{-1}$)

ethylbenzene + •CH_3 = toluene + n-•C_4H_9	4.53×10^2	2.542	11322
ethylbenzene + •C_3H_5 = allylbenzene + n-•C_4H_9	1.06×10^5	2.192	25304

The kinetic model includes the reversible H-transfers between every radical and *n*-butylbenzene, and between the main radicals and the main products. Transfer of aromatic H atoms was not considered. Most of the kinetic parameters were computed on the basis of structure-reactivity correlations by the EXGAS software [35] or taken by analogy with kinetic parameters of similar reactions. The kinetic parameters of some very sensitive reactions (Table 3) were computed by theoretical calculations at the CBS-QB3 level of theory. Because of the large size of the system *n*-butylbenzene + abstracting radical (C_{6+}), model compounds were used for the computations while respecting the nature of the H transferred: for allylic H, 1-butene was considered, for secondary H on alkyl group, propane was considered and ethane for primary H. This approach led to the set of H-abstraction rate rules given in Table 3.

Table 3. Kinetic parameters of sensitive H-transfers calculated by theoretical calculations at the CBS-QB3 level of theory (C_6H_5# stands for the aromatic cycle).

RH + X• ⇆ R• + XH	A ($cm^3.mol^{-1}.s^{-1}$)	n	E ($cal.mol^{-1}$)
X• = Phenyl radical			
Allylic H	2.30×10^1	3.621	-860
Secondary alkylic H	4.66×10^0	3.950	800
Primary alkylic H	1.16×10^{-1}	4.187	4380
X• = Benzyl radical			
Allylic H	1.89×10^{-1}	3.931	9740
Secondary alkylic H	7.36×10^{-1}	3.983	15060
Primary alkylic H	3.50×10^{-1}	3.963	18550
X• = C_6H_5#$CHCH_3$			
Allylic H	1.12×10^{-2}	4.226	10240
Secondary alkylic H	9.11×10^{-2}	4.208	16310
Primary alkylic H	1.64×10^{-1}	4.146	20070

X• = C_6H_5#CH_2CH_2			
Allylic H	1.88×10^{-2}	4.299	4150
Secondary alkylic H	6.18×10^{-3}	4.556	7540
Primary alkylic H	1.29×10^{-3}	4.622	9880

The unimolecular isomerization reactions of phenylbutyl radicals through 4- and 5-centers cyclic transition states were included in the mechanism with their kinetic parameters computed by theoretical calculations (Table 4). Note that the internal H-transfers of aromatic H-atoms were neglected.

Table 4. Kinetic parameters for unimolecular isomerizations of phenylbutyl radicals calculated by theoretical calculations at the CBS-QB3 level of theory.

Reaction	A (s^{-1})	n	E ($cal.mol^{-1}$)
C_6H_5#CH˙$CH_2CH_2CH_3$ = C_6H_5#CH_2CH_2CH˙CH_3	9.11×10^{2}	2.834	40730
C_6H_5#CH_2CH˙CH_2CH_3 = C_6H_5#$CH_2CH_2CH_2CH_2$˙	1.18×10^{1}	3.526	33950
C_6H_5#CH˙$CH_2CH_2CH_3$ = C_6H_5#$CH_2CH_2CH_2CH_2$˙	3.19×10^{4}	2.169	27750

Reactions of the first two rows involve 4-center cyclic transition state (TS) structures, while the one in the last row is a 5-center ring TS. At 500 K, the latter reaction's rate is at least two orders of magnitude higher than the ones involving 4-center TS.

The reversible decompositions by β-scission of C-C bonds of every radical except those involving aromatic C-C bonds were included, as well as β-scissions of C-H bonds when they lead to resonance-stabilized compounds. The kinetic parameters were calculated by theoretical methods at the CBS-QB3 level of theory or taken by analogy with similar reactions. The kinetic parameters for the decompositions by β-scission of phenylbutyl radicals are presented in Table 5.

Table 5. Computed kinetic parameters for the decompositions by β-scission of phenylbutyl radicals at the CBS-QB3 level of theory.

Reaction	A (s^{-1})	n	E ($cal.mol^{-1}$)
$C_6H_5\#CH^{\cdot}CH_2CH_2CH_3 = styrene + C_2H_5^{\cdot}$	1.23×10^{14}	0.257	36370
$C_6H_5\#CH_2CH^{\cdot}CH_2CH_3 = 1\text{-butene} + phenyl$	1.28×10^{12}	0.722	39410
$C_6H_5\#CH_2CH^{\cdot}CH_2CH_3 = allylbenzene + CH_3^{\cdot}$	2.45×10^{11}	0.811	29740
$C_6H_5\#CH_2CH_2CH^{\cdot}CH_3 = propene + benzyl$	1.25×10^{10}	0.992	21480
$C_6H_5\#CHCH_2CH_2CH_2^{\cdot} = C_2H_4 + C_6H_5\#CH_2CH_2^{\cdot}$	2.63×10^{12}	0.375	28860

The ring-closure reactions (Fig. 6) were also considered, since tetraline, methylindane and indane were found among the products. The kinetic parameters were taken from Kislov et al. [36] for indane-type species, and were calculated at the CBS-QB3 level of theory for tetraline-type species (Table 6).

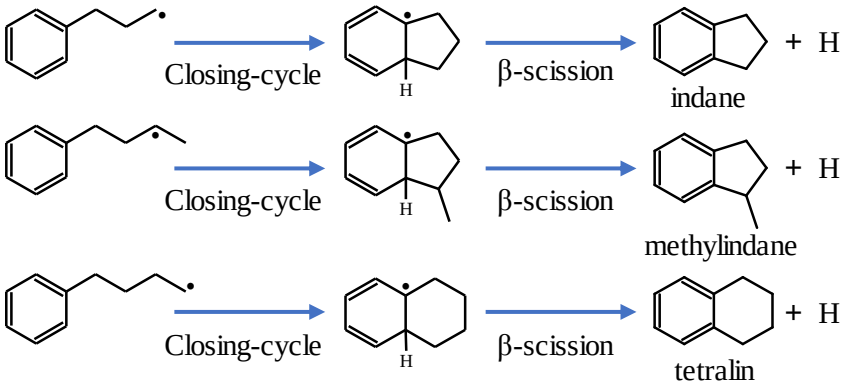

Figure 6. Ring-closure reactions.

Table 6. Kinetic parameters for ring-closure reactions.

Reaction	A (s^{-1})	n	E ($cal.mol^{-1}$)
Indane-type			
Ring-closure	2.41×10^{11}	0	17940
β-scission	7.45×10^{9}	1.035	22900
Tetraline-type			
Ring-closure	8.30×10^{5}	1.110	9870
β-scission	9.84×10^{10}	0.833	28830

The retroene reaction for *n*-butylbenzene (Fig. 7) was considered because a previous study showed that it could contribute to the consumption of alkylbenzene ([14], [18] and [22]). This reaction consists of an intramolecular H-transfer and a reorganization of the electron pairs. Two H atoms can be transferred, so the kinetic parameters were calculated at the CBS-QB3 level of theory in both cases, and then the global kinetic parameters were deduced (Table 7).

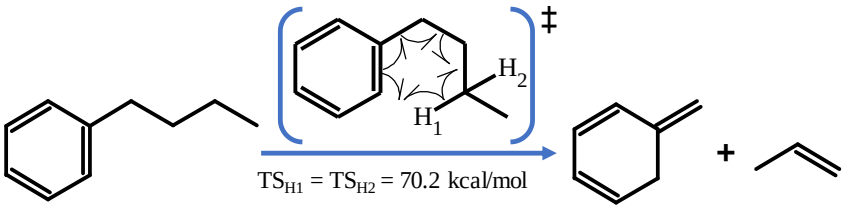

Figure 7. Retroene reaction for *n*-butylbenzene (TS stands for Transition State).

Table 7. Kinetic parameters for retroene reaction of *n*-butylbenzene computed at the CBS-QB3 level of theory (mol, cm^3, s, cal).

Reaction	A (s^{-1})	n	E ($cal.mol^{-1}$)
TS_{H1}	1.05×10^6	1.824	68160
TS_{H2}	1.58×10^6	1.819	68060
global	**2.62×10^6**	**1.822**	**68100**

5-methyl-1,3-cyclohexadiene is transformed to toluene by intramolecular H-transfer. The kinetic parameters were taken from NIST kinetics database [37]. The computed energy barrier height is higher than that estimated in previous studies ([18] and [22]).

Some terminations by recombination and disproportionation are implicitly included in the reversible initiations. In the primary mechanism, the combinations of the benzylic butylbenzyl radical (C_6H_5#CH•$CH_2CH_2CH_3$) with CH_3, C_2H_5, C_3H_5 and *n*-C_4H_9 radicals were included. Combinations of the primary radicals created in the initial C-C bond dissociations and in the β-scissions were also included. Associated kinetic parameters were taken from EXGAS's rate rules [35].

4.2.2. *n*-ary mechanisms

The comprehensive primary mechanism was used to perform preliminary simulations on a large scale of temperature and pressure conditions to identify the main secondary products and the free radicals featuring the highest molar fractions. This approach was used to limit the combinatory explosion that would occur if all the possible reactions were to be included in the mechanism. Based on this species selection method, it was observed that allylbenzene, styrene, toluene and propene were the main primary products. For these compounds, the same systematic decomposition reactions as those detailed above for *n*-butylbenzene were included. As these compounds are unsaturated, the addition reactions of the radicals in the highest concentration in the preliminary simulations were included: ethyl, *n*-butyl, allyl, phenyl, benzyl and 1-phenylbutyl radicals. The decomposition reactions of the formed adducts follow the mechanism development rules set in the primary mechanism, *i.e.*, H-abstractions from *n*-butylbenzene, isomerizations, β-scissions, ring-closures.

The same procedure (preliminary simulations with the primary and secondary model, species selection and addition of a new decomposition sub-mechanism) was iteratively performed for the development of subsequent *n*-ary sub-mechanisms. The main molecules appearing in these procedures are given in Figure 8.

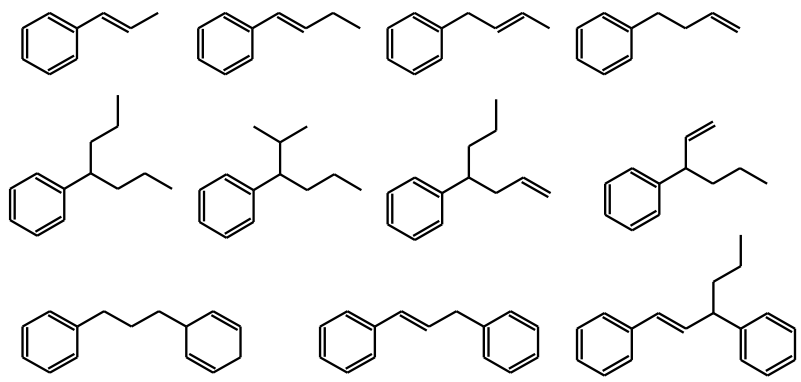

Figure 8. Principal n-ary molecules chosen by the iterative selection procedure.

As the size of molecules in the mechanism rapidly grows with each new *n*-ary mechanism, the iterations were stopped when the model was able to reproduce the experimentally identified molecules featuring the largest size.

4.3. Validation

Simulations with the kinetic model were performed using the software package CHEMKIN II [26], and SENKIN at constant pressure and temperature. It should be noted that this software uses the ideal gas law to calculate concentrations. Obviously, the ideal gas law is not valid at high pressure. That is why the initial concentration was first calculated separately by using the Peng-Robinson equation of state [38], which is implemented in the software DIAGSIM [39].

Figure 9 presents the comparison between the experimental conversion (symbols) and the simulation results (solid lines). A good agreement between the experiments and the model is obtained in the whole range of temperature and conversion.

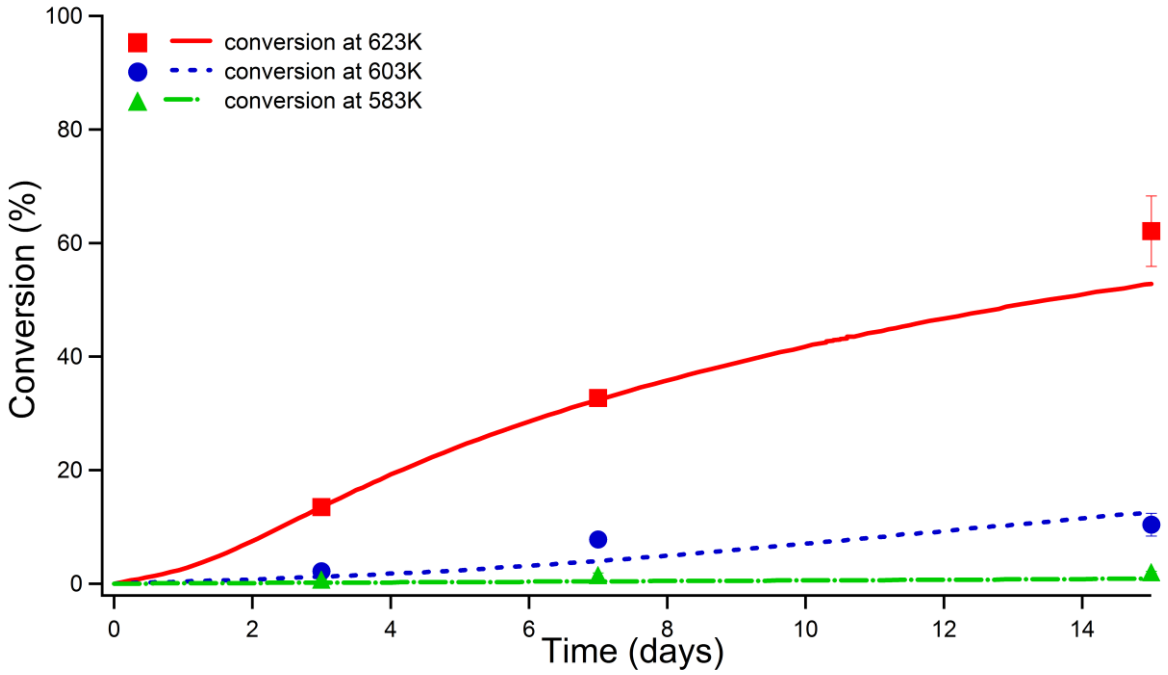

Figure 9. Comparison between experimental conversions (symbols) and simulation results (solid lines) for the pyrolysis of *n*-butylbenzene at 583, 603, 623 K and 70 MPa.

Figures 10 and 11 present the comparison between the experimental ratios X_i and the simulated mole fractions x_i for the gases. Overall, a good agreement is observed for methane, ethane (except at 603 K) and propane, which are the major products. The results are also satisfying for *n*-butane which is a minor product. It should be noted that the kinetic model predicts the production of small amounts of propylene, in agreement with [18] and [22], but propylene was not detected in our experiments. If propylene is co-eluting with propane, we should add the simulation result of propane to that of

propylene and compare it with the experimental results of the co-eluted peak. This leads to a small overestimation of the propane-propylene profile (not represented here) from the kinetic model, in comparison to the experimental result.

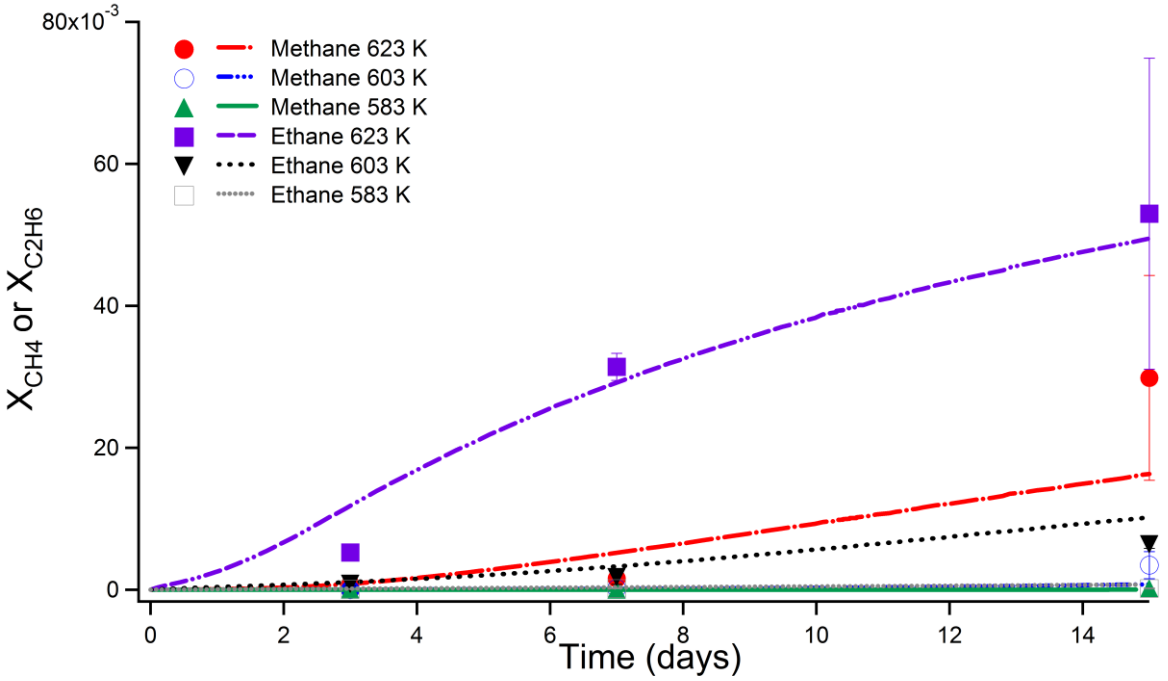

Figure 10. Comparison between experimental molar fractions (symbols) and simulation results (solid lines) for methane and ethane after pyrolysis of *n*-butylbenzene at 583, 603, 623 K and 70 MPa.

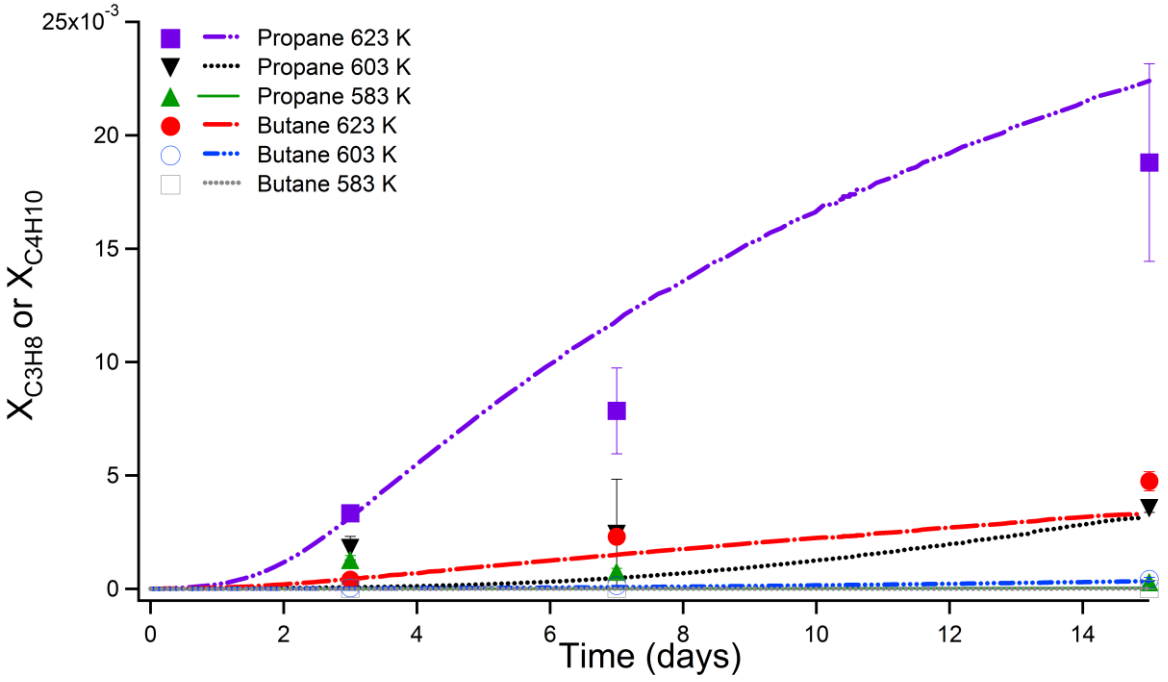

Figure 11. Comparison between experimental molar fractions (symbols) and simulation results (solid lines) for propane and butane after pyrolysis of *n*-butylbenzene at 583, 603, 623 K and 70 MPa.

Figures 12 and 13 present the comparison between the experimental ratios X_i and the simulated mole fractions x_i for the other main products: toluene, ethylbenzene, iso-butylbenzene, iso-heptylbenzene (sums of the isomers) and methylindane.

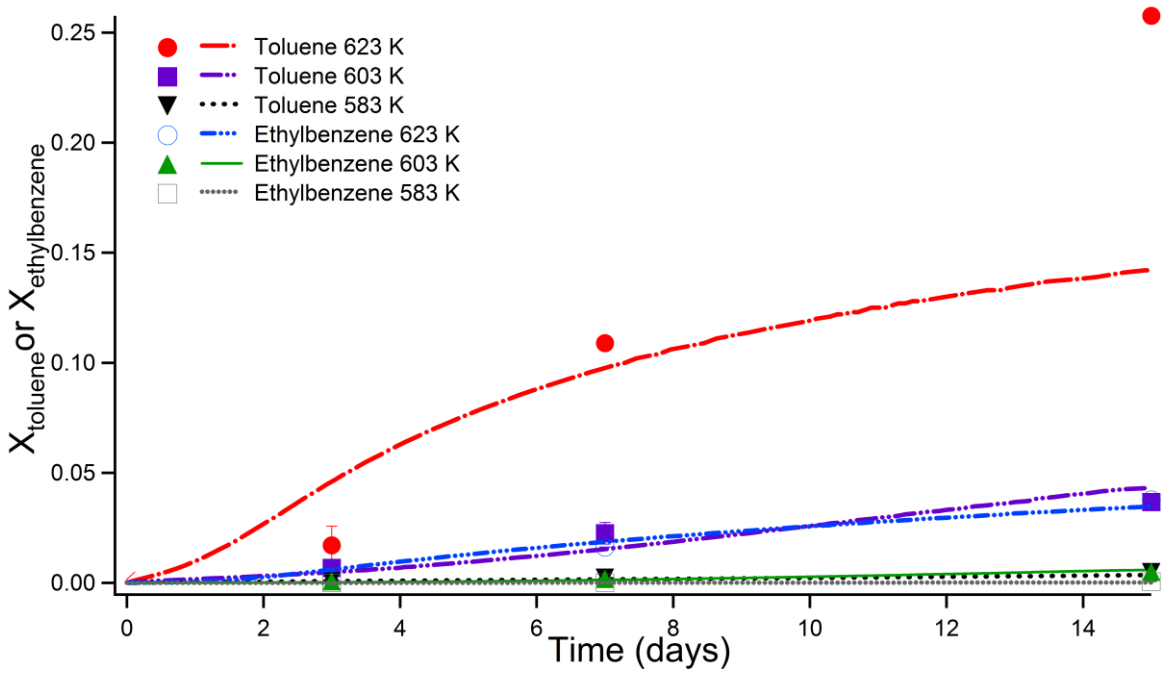

Figure 12. Comparison between experimental molar fractions (symbols) and simulation results (solid lines) for toluene and ethylbenzene after pyrolysis of *n*-butylbenzene at 583, 603, 623 K and 70 MPa.

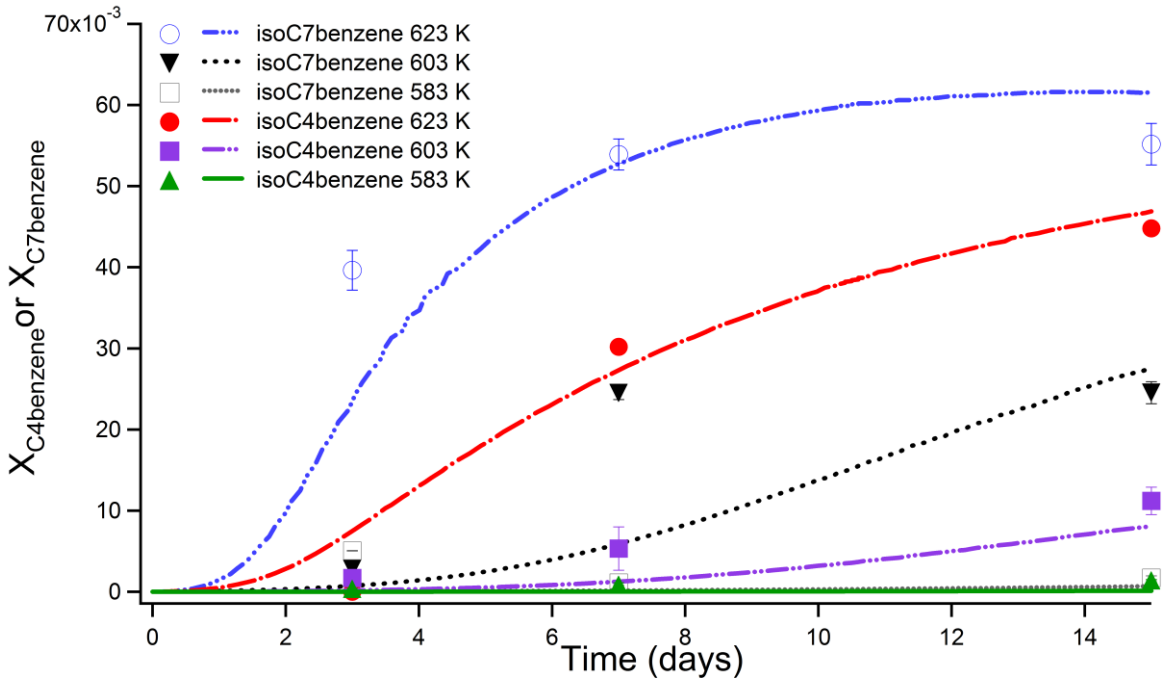

Figure 13. Comparison between experimental molar fractions (symbols) and simulation results (solid lines) for iso-butylbenzene and iso-heptylbenzene (sums of the isomers) after pyrolysis of *n*-butylbenzene at 583, 603, 623 K and 70 MPa.

A very good agreement is obtained for toluene (except at very high conversion), ethylbenzene, iso-butylbenzene (sum of the isomers) and iso-heptylbenzene (sum of isomers). The discrepancies observed for toluene at 623 K could be related to the difficulty to measure it at high concentration, due to column and peak saturation. For this reason, toluene at 623K and 15 days was not measured by Thermodesorption-GC-FID, but in the same way as the remaining quantity of butylbenzene. The measurement could not be duplicated, which could explain the high deviation in comparison to the simulation result.

Comparisons between experiments and simulation were also performed for some minor products, *i.e.* styrene and butenylbenzene (sum of the isomers) (Fig.14) and methylindane (Fig.15). The order of magnitude is well represented by the model under all conditions, but some discrepancies are observed which could be due to the difficulty to precisely measure very low concentrations. In the case of

styrene, the discrepancies could indicate that some additions of radicals to styrene are missing or are under-evaluated.

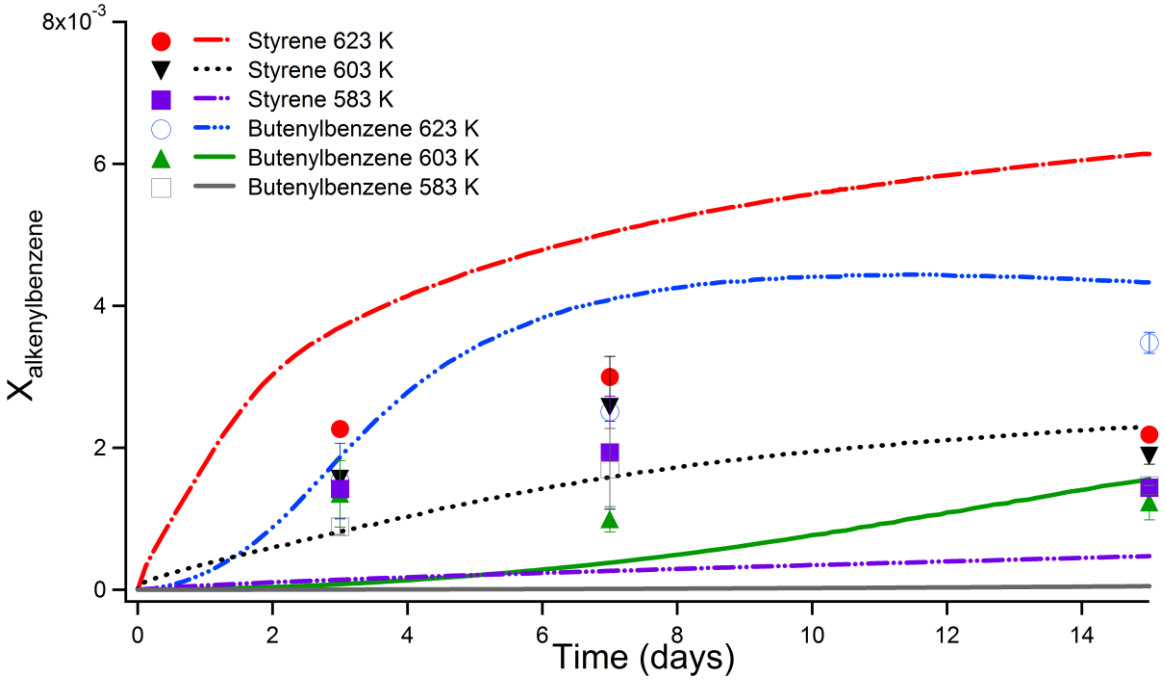

Figure 14. Comparison between experimental molar fractions (symbols) and simulation results (solid lines) for styrene and butenylbenzene (sum of the isomers) after pyrolysis of *n*-butylbenzene at 583, 603, 623 K and 70 MPa.

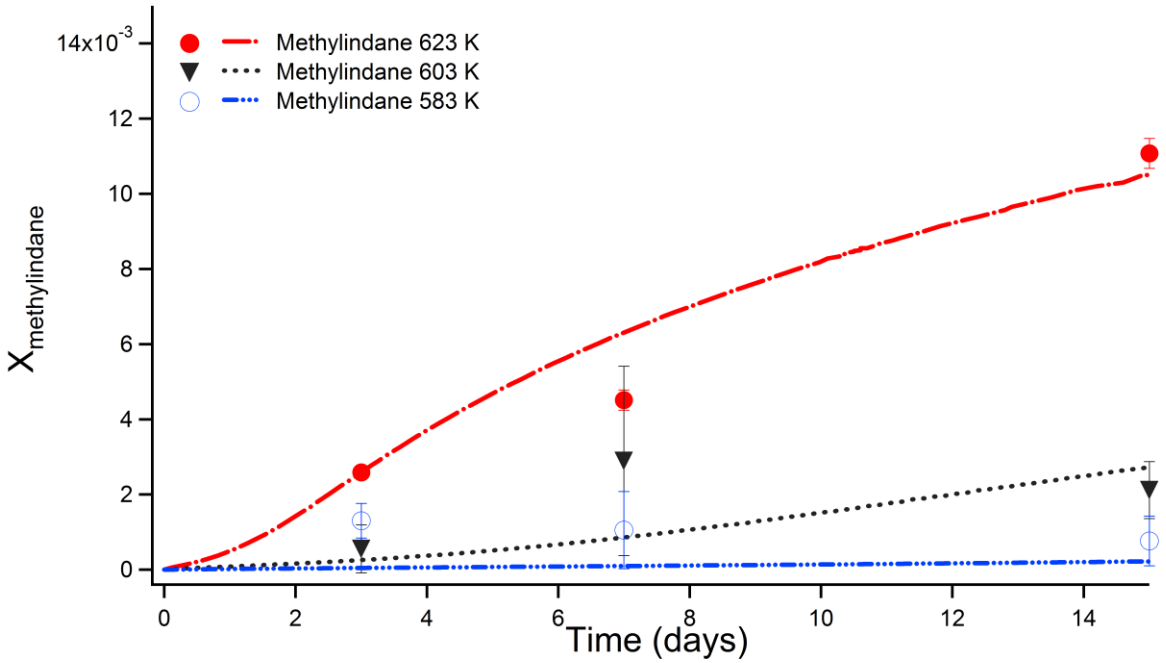

Figure 15. Comparison between experimental molar fractions (symbols) and simulation results (solid lines) for methylindane (sum of the isomers) after pyrolysis of *n*-butylbenzene at 583, 603, 623 K and 70 MPa.

The experimental and simulation selectivity has also been compared at 603 K for the main products (Supplementary Material 5). The agreement between experimental and simulation results is very satisfying for every liquid product except isoheptylbenzene which is under-estimated. Discrepancies are observed for gaseous products (except butane), which is probably related to the difficulty to precisely measure their amount.

4.4. Flux analysis

The model was used to highlight the main reaction pathways in the pyrolysis of *n*-butylbenzene. A flux analysis was performed at 623 K, 70 MPa and 52% conversion (Fig. 16). The flux corresponds to the ratio between the rate of the studied pathway and the consumption rate of the considered species, in percentage. The flux analysis shows that *n*-butylbenzene is mainly consumed by H-transfers (98%) leading to 1-phenyl-but-1-yl (PHC4H8-1) and 1-phenyl-but-3-yl (PHC4H8-3) radicals. This is in agreement with the flux analysis of Carr et al. [22] who calculated that H-transfers represent 92% of the *n*-hexylbenzene consumption at 673 K and 7.4 MPa.

The 1-phenyl-but-3-yl (PHC4H8-3) radicals mainly react (90%) through decomposition by β-scission to yield propylene and benzyl radicals, which leads to toluene by H-transfers and bibenzyl by termination. The 1-phenyl-but-3-yl (PHC4H8-3) radicals also react (10%) by ring-closure reactions which yield methylindane.

The 1-phenylbut-1-yl (PHC4H8-1) radicals mainly react 1) through decomposition by β-scission (17%) yielding styrene and ethyl radicals, 2) by addition to propene (39%) which yields phenylheptyl (IM7 and IM8) radicals, 3) by addition to alkenylbenzenes (styrene, PHCHCHCH3, PHC4H7Z1, PHC4H7Z2) (23%) which leads to biaromatic (Im-biAr9, Im-biAr16, IM50, IM75) radicals. It should be noted that at lower pressure and higher temperature ([15] and [22]), the additions of radicals to

alkenes are not depicted as important reactions on the contrary to our results. The conclusion is the same for ring-closure reactions and ipso-additions which are rather important in our study but not described at lower pressure and higher temperature ([15] and [22]).

The flux analysis for the decomposition reactions of the biaromatic radicals is presented in Appendix 1. It highlights: 1) the main formation pathways of iso-heptylbenzenes (C13H20-1) and iso-butylbenzenes (PHiC4H9) which belong to the major products, 2) the main reaction pathways leading to ethylbenzene which is also an important product. Ethylbenzene is produced by H-transfer of phenylethyl radicals, which are produced by β-scission decomposition of the biaromatic radical formed by addition of 1-phenylbut-1-yl radical to styrene. This pathway (showed in the Appendix 1) has not been described before, only the Reverse Radical Disproportionation between styrene and the alkylbenzene, that does not appear in Figure 16 but is taken into account in the model ([18] and [22]).

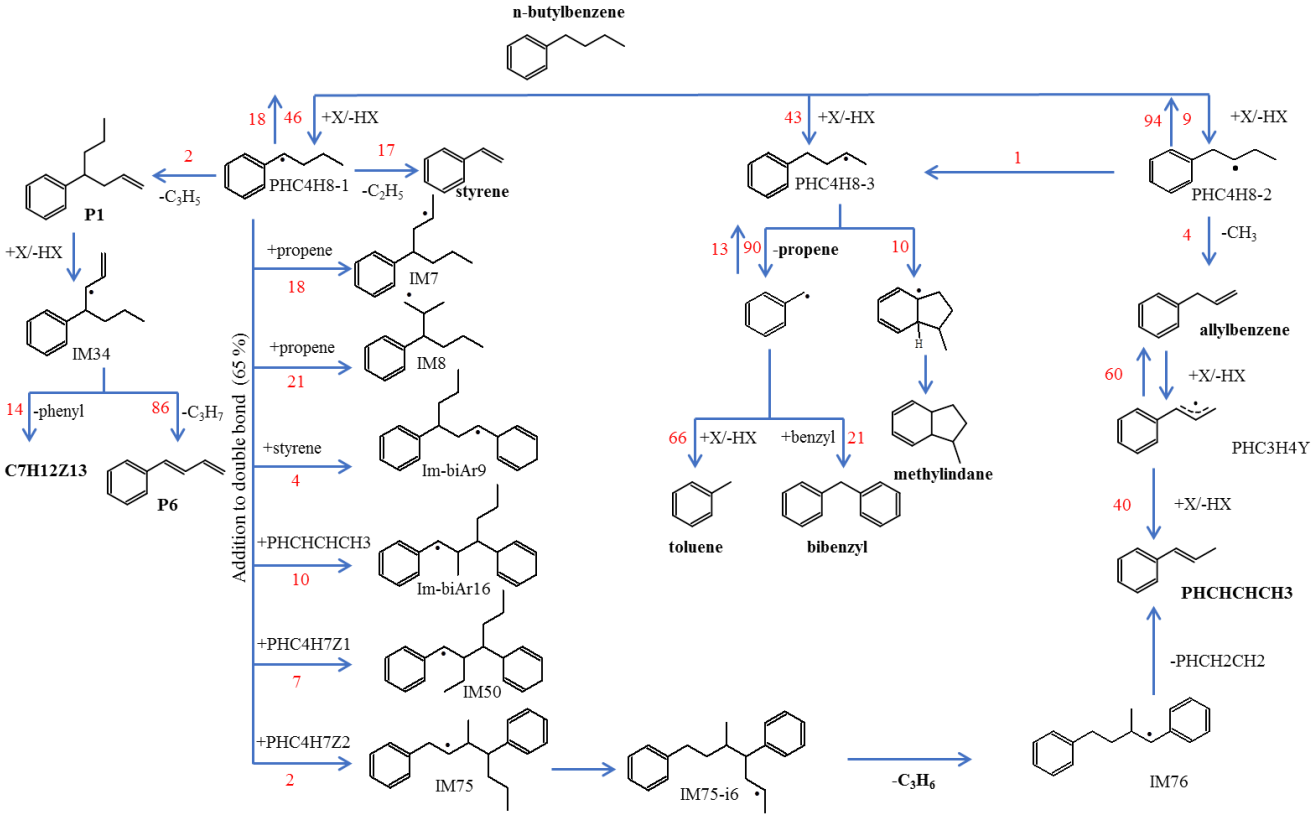

Figure 16. Flux analysis of the *n*-butylbenzene pyrolysis (673 K, 70 MPa, 52% conversion).

Concerning the formation pathways of methane, ethane and propane, they are produced by H-transfers to methyl, ethyl and propyl radicals which come from decomposition by β-scission. The formation pathway of *n*-butane is different: it derives from the butyl radical which is produced by ipso-addition of radicals (especially propen-3-yl radicals) to *n*-butylbenzene.

5. Apparent kinetic parameters

The apparent kinetic parameters were computed at 623 K. Simulations were performed and reached up to 30% conversion. The consumption rates *r* were computed by CHEMKIN at 30% conversion and by plotting *ln r vs -1/RT* (where *R* is the ideal gas constant and *T* the temperature in K) with *T* = 621, 623 and 625 K. The slope of the graph corresponds to the apparent E_a found equal to 66.6 kcal.mol^{-1}. This apparent E_a is consistent with the value computed from the kinetic model of the thermal cracking of decylbenzene at 673 K and 70 MPa (67 kcal.mol^{-1}) [40]. It is also very similar to the experimental value (65 kcal.mol^{-1}) of Leigh and Szwarc [41] for *n*-butylbenzene, although the pressure-temperature conditions were not specified in their paper. The experimental values of Freund and Olmstead (52.9 kcal.mol^{-1}) [42] and Yu and Eser (57 kcal.mol^{-1}) [43] for *n*-butylbenzene are lower than the apparent E_a computed in this work, but both teams worked at higher temperature and lower pressure than those studied here. Behar et al. [12] also found a rather low apparent E_a (53.3 kcal.mol^{-1}) for *n*-dodecylbenzene, as well as Savage and Klein [15] for *n*-pentadecylbenzene (55.5 kcal.mol^{-1}). The lower pressure, higher temperature and longer side-chain of the alkylbenzene complicate the comparison with our results.

The pseudo-first-order kinetic law ($r = k \times c$, with *k* the rate constant following the Arrhenius law, *k* in s^{-1} and *c* in mol.m^{-3}) leads to:

$$\ln r = \ln A - E_a/RT + \ln c$$

The Y-intercept of the plots *ln r vs -1/RT* allows the calculation of *A*, which was determined as 6.3×10^{16} s^{-1}. This value is almost of the same order of magnitude as the experimental value of Yu and Eser (4×10^{17} s^{-1}) [43]. It is lower than the previous *A* computed from the kinetic model of *n*-

decylbenzene (1.2×10^{18}) [40], but this is consistent with a longer side-chain, which increases the reaction pathways.

6. Extrapolation to low temperature (473 K)

The detailed kinetic model constructed in this paper was then applied to simulate geological conditions of pressure and temperature, *i.e.* 473 K and 700 MPa characteristic of deeply buried hydrocarbon reservoirs.

At these conditions, the main products remain approximately the same as at higher temperature, except that alkenes and alkenylbenzenes become negligible at low temperature. This is due to the additions of radicals to double bonds, whose importance increases at low temperature because their activation energy is particularly low in comparison to the other elementary reactions.

The half-life of *n*-butylbenzene at 473 K is about 5 million years. This value is about the same as the half-life of the alkanes, which is between 4 and 5 million years, depending on the chain length [40]. But the half-life of *n*-butylbenzene is lower than that of toluene (20 million years [40]) and greater than that of *n*-decylbenzene (0.7 million years [40]). This sequence is consistent with the increase of reactivity with the length of the side-chain.

7. Conclusion

The thermal cracking of *n*-butylbenzene was experimentally studied at high pressure (70 MPa), moderate temperature (583, 603 and 623 K) and for durations of 3, 7 and 15 days. The pyrolysis was performed in sealed gold tubes in isobaric regime. At these conditions, the conversion of *n*-butylbenzene varied between 0.7% and 62%. Three main chemical families were observed: short alkylbenzenes (mostly toluene and ethylbenzene), branched alkylbenzenes (isomers of iso-butylbenzene and iso-heptylbenzene) and short alkanes (from CH_4 to C_4H_{10}). As minor products, alkenylbenzenes (styrene and butenylbenzene), methylindane and diaromatic structures were also detected.

A detailed kinetic model composed of 3542 free-radical reactions and 383 species (molecules and free-radicals) was written in a systematic manner by taking into account all relevant elementary free-

radical reactions. The thermochemical and kinetic parameters of the most important decomposition pathways were computed by theoretical calculations, which increase the robustness of our kinetic model. A very good agreement between experiments and simulations was observed for most major and minor compounds.

The apparent kinetic parameters of the thermal decomposition of *n*-butylbenzene were computed by the kinetic model under the assumption of a first-order global rate law: the apparent activation energy was found equal to 66.6 kcal.mol^{-1} and the frequency factor to 6.3×10^{16} s^{-1}. The extrapolation to low temperature (473 K), which is characteristic of deeply buried oil reservoirs, shows that the stability of *n*-butylbenzene is about the same as of alkanes, but *n*-butylbenzene is more stable than *n*-decylbenzene and less stable than toluene.

The next step of this study will be the pyrolysis of *n*-butylbenzene with H_2S in order to study the potential acceleration or inhibition effect of H_2S on *n*-butylbenzene pyrolysis, as well as to highlight some formation pathways of organosulfur compounds in geological oil reservoirs.

Acknowledgements. This work was supported by ICEEL (Institut Carnot pour l'Energie et l'Environnement en Lorraine). This work was granted access to the HPC resources of IDRIS under the allocation 2017-A0010807249 made by GENCI.

Supplementary Materials.

1) Yield and selectivity of the major products
2) Mechanism in the CHEMKIN format
3) Nomenclature of the species
4) Geometries of the Transition States.
5) Comparison between the experimental and simulation selectivity of the major products at 603K.

List of table captions

Table 1. Conversion and mass balance of pyrolysis of butylbenzene.

Table 2. Kinetic parameters of the ipso-additions estimated by theoretical calculations at the CBS-QB3 level of theory (mol, cm^3, s, cal).

Table 3. Kinetic parameters of sensitive H-transfers calculated by theoretical calculations at the CBS-QB3 level of theory (C_6H_5# stands for the aromatic cycle).

Table 4. Kinetic parameters for unimolecular isomerizations of phenylbutyl radicals estimated by theoretical calculations at the CBS-QB3 level of theory.

Table 5. Kinetic parameters for decompositions by β-scission of phenylbutyl radicals estimated by theoretical calculations at the CBS-QB3 level of theory.

Table 6. Kinetic parameters for ring-closure reactions.

Table 7. Kinetic parameters for retroene reaction of butylbenzene estimated by theoretical calculations at the CBS-QB3 level of theory.

List of figure captions

Figure 1. Schematic diagram of the oven containing the piercing device for the gold cells and the GC-FID.

Figure 2. Example of GC-FID-chromatogram obtained after pyrolysis of *n*-butylbenzene at 623K, 70 MPa, during 15 days (59% conversion).

Figure 3. Bond Dissociation Energies of *n*-butylbenzene at 298 K (kcal.mol^{-1}).

Figure 4. Bimolecular initiations between 2 molecules of *n*-butylbenzene (CBS-QB3 enthalpies of reaction at 298 K, in kcal.mol^{-1}).

Figure 5. Ipso-addition of radicals to *n*-butylbenzene.

Figure 6. Ring-closure reactions.

Figure 7. Retroene reaction for *n*-butylbenzene (TS stands for Transition State).

Figure 8. Principal *n*-ary molecules chosen by the iterative selection procedure.

Figure 9. Comparison between experimental conversions (symbols) and simulation results (solid lines) for the pyrolysis of *n*-butylbenzene at 583, 603, 623 K and 70 MPa.

Figure 10. Comparison between experimental molar fractions (symbols) and simulation results (solid lines) for methane and ethane for the pyrolysis of *n*-butylbenzene at 583, 603, 623 K and 70 MPa.

Figure 11. Comparison between experimental molar fractions (symbols) and simulation results (solid lines) for propane and butane for the pyrolysis of *n*-butylbenzene at 583, 603, 623 K and 70 MPa.

Figure 12. Comparison between experimental molar fractions (symbols) and simulation results (solid lines) for toluene and ethylbenzene for the pyrolysis of *n*-butylbenzene at 583, 603, 623 K and 70 MPa.

Figure 13. Comparison between experimental molar fractions (symbols) and simulation results (solid lines) for iso-butylbenzene and iso-heptylbenzene (sum of the isomers) for the pyrolysis of *n*-butylbenzene at 583, 603, 623 K and 70 MPa.

Figure 14. Comparison between experimental molar fractions (symbols) and simulation results (solid lines) for styrene and butenylbenzene (sum of the isomers) for the pyrolysis of *n*-butylbenzene at 583, 603, 623 K and 70 MPa.

Figure 15. Comparison between experimental molar fractions (symbols) and simulation results (solid lines) for methylindane (sum of the isomers) for the pyrolysis of *n*-butylbenzene at 583, 603, 623 K and 70 MPa.

Figure 16. Flux analysis of the *n*-butylbenzene pyrolysis (673 K, 70 MPa, 58% conversion).

APPENDIX 1: The flux analysis for the decomposition reactions of the biaromatic radicals (623 K, 70 MPa, 52% conversion)

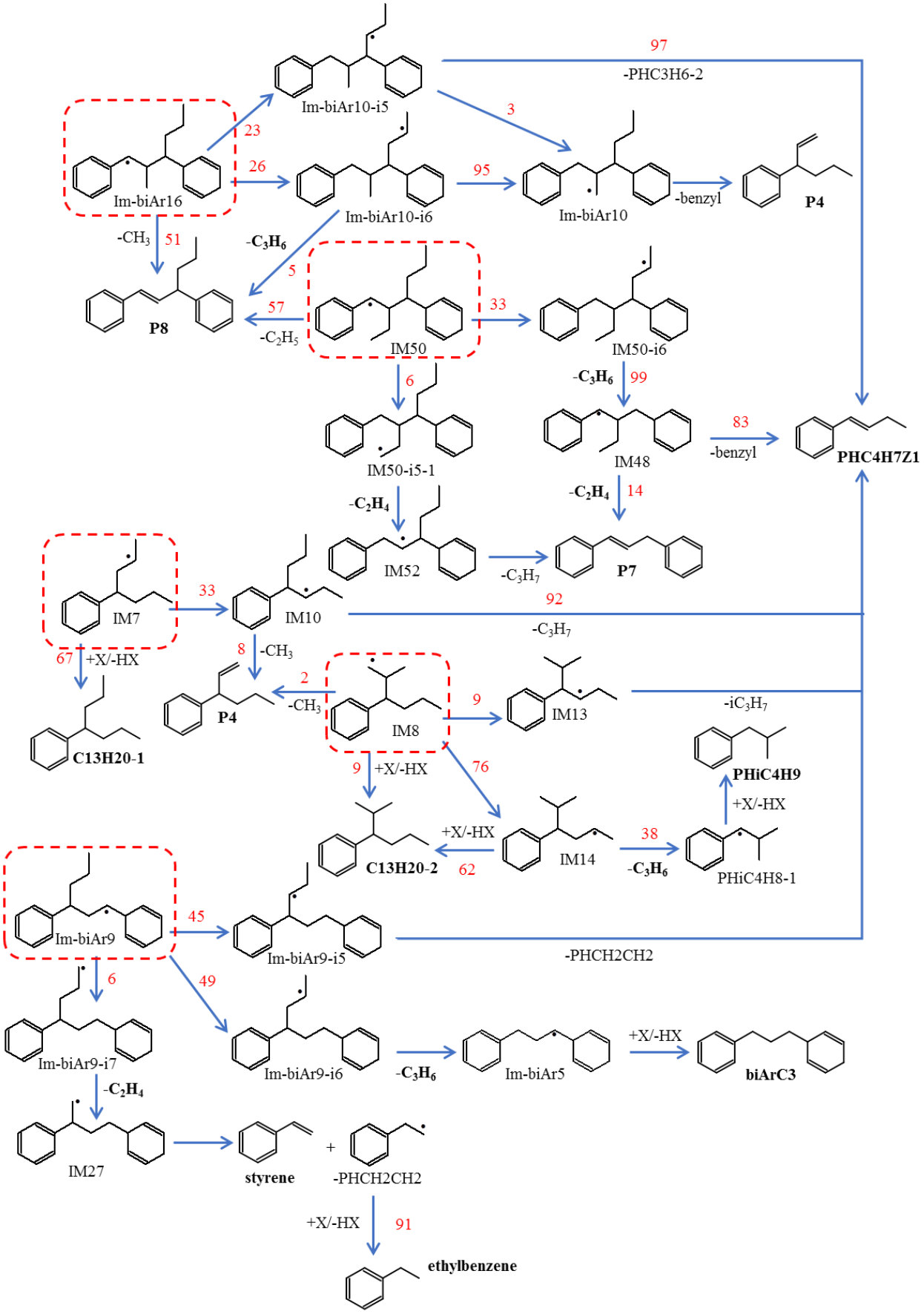

REFERENCES

[1] P. Ungerer, R. Pelet, Extrapolation of the kinetics of oil and gas formation from laboratory experiments to sedimentary basins, Nature 327 (1987) 52-54.

[2] P. Ungerer, F. Béhar, M. Villalba, O.R. Heum, A. Audibert, Kinetic modelling of oil cracking, Org. Geochem. 13 (1988) 857-868.

[3] A. K. Burnham, Global Chemical Kinetics of Fossil Fuels – How to Model Maturation and Pyrolysis, Springer, 2017.

[4] F. Béhar, S. Kressmann, J.L. Rudkiewicz, M. Vandenbroucke, Experimental simulation in a confined system and kinetic modelling of kerogen and oil cracking, Org. Geochem. 19 (1992) 173–189.

[5] F. Béhar, M. Vandenbroucke, Y. Tang, F. Marquis, J. Espitalié, Thermal cracking of kerogen in open and closed systems: determination of kinetic parameters and stoichiometric coefficients for oil and gas generation, Org. Geochem. 26 (1997) 321–339.

[6] F. Béhar, F. Lorant, L. Mazeas, Elaboration of a new compositional kinetic schema for oil cracking, Org. Geochem. 39 (2008) 764-782.

[7] F. Béhar, H. Budzinski, M. Vandenbroucke, Y. Tang, Methane Generation from Oil Cracking: Kinetics of 9-Methylphenanthrene Cracking and Comparison with Other Pure Compounds and Oil Fractions, Energy Fuels 13 (1999) 471-481.

[8] F. Béhar, M. Vandenbroucke, Experimental Determination of the Rate Constants of the n-C25 Thermal Cracking at 120, 400, and 800 bar: Implications for High-Pressure/High-Temperature Prospects, Energy Fuels 10 (1996) 932-940.

[9] D. Rakotoalimanana, F. Béhar, R. Bounaceur, V. Burklé-Vitzthum, P-M. Marquaire, Thermal cracking of n-butylcyclohexane at high pressure (100 bar) – part 1: experimental study, J. Anal. Appl. Pyrolysis, 117 (2016) 1-16.

[10] D. Rakotoalimanana, R. Bounaceur, F. Béhar, V. Burklé-Vitzthum, P-M. Marquaire, Thermal cracking of n-butylcyclohexane at high pressure (100 bar) – part 2: Mechanistic modeling, J. Anal. Appl. Pyrolysis, 120 (2016) 174-185.

[11] B. P. Tissot, D.H. Welte, Petroleum Formation and Occurrence, 2nd Edition, Springer-Verlag, 1984.

[12] F. Béhar, F. Lorant, H. Budzinski, E. Desavis, Thermal Stability of Alkylaromatics in Natural Systems: Kinetics of Thermal Decomposition of Dodecylbenzene, Energy Fuels 16 (2002) 831-841.

[13] J-P. Leininger, F. Lorant, C. Minot, F. Béhar, Mechanisms of 1-methylnaphthalene pyrolysis in a batch reactor, Energy Fuels 20 (2006) 2518-2530.

[14] F. Dominé, High pressure pyrolysis of n-hexane, 2,4-dimethylpentane and 1-phenylbutane. Is pressure an important geochemical parameter? Org. Geochem. 17 (1991) 619-634.

[15] P.E. Savage, M.T. Klein, Asphaltene Reaction Pathways. 2. Pyrolysis of n-Pentadecylbenzene, Ind. Eng. Chem. Res. 26 (1987) 488-494.

[16] P. C. Mandal, T. Shiraishi, Wahyudiono, M. Sasaki, M. Goto, Kinetics and Reaction Pathways for Heptylbenzene Decomposition in Supercritical Water, J. Chem. Eng. of Japan 44 (7) (2011) 486-493.

[17] R. Bounaceur, G. Scacchi, P-M. Marquaire, F. Dominé, Mechanistic modeling of the thermal cracking of tetralin, Ind. Eng. Chem. Res. 39 (2000) 4152-4165.

[18] V. Burklé-Vitzthum, R. Michels, G. Scacchi, P-M. Marquaire, Mechanistic Modeling of the Thermal Cracking of Decylbenzene, Ind. Eng. Chem. Res. 23 (2003) 5791-5808.

[19] L. Fusetti, F. Béhar, R. Bounaceur, P-M. Marquaire, K. Grice, S. Derenne, New insights into secondary gas generation from the thermal cracking of oil: Methylated aromatics. A kinetic approach using 1,2,4-trimethylbenzene. Part I: A mechanistic model, Org. Geochem. 41 (2010) 146-167.

[20] F. Lannuzel, R. Bounaceur, R. Michels, G. Scacchi, P-M. Marquaire, An extended mechanism including high pressure conditions (700 bar) for toluene pyrolysis, J. Anal. Appl. Pyrolysis 87 (2010) 236-247.

[21] R. Bounaceur, J.F. Leininger, F. Lorant, P-M. Marquaire, V. Burklé-Vitzthum, Kinetic modeling of 1-Methylnaphthalene pyrolysis at high pressure (100 bar), J. Anal. Appl. Pyrolysis 124 (2017) 542-562.

[22] A. G. Carr, C. A. Class, L. Lai, Y. Kida, T. Monrose, W. H. Green, Supercritical Water Treatment of Crude oil and Hexylbenzene: An Experimental and Mechanistic Study on Alkylbenzene Decomposition, Energy Fuels 29 (2015) 5290-5302.

[23] P. Landais, R. Michels, B. Poty, Pyrolysis of organic matter in cold-seal autoclaves. Experimental approach and application, J. Anal. Appl. Pyrolysis 16 (2) (1989) 103-115.

[24] R. Michels, P. Landais, Artificial coalification – comparison of confined pyrolysis and hydrous pyrolysis, Fuel 73 (11) (1994) 1691-1696.

[25] M. Monthioux, P. Landais, J.C. Monin, Comparison between natural and artificial maturation series of humic coals from the Mahakam delta, Indonesia. Org. Geochem. 8 (4) (1985) 275-292.

[26] R.J. Kee, F.M. Rupley, J.A. Miller, Chemkin-II: A Fortran chemical kinetics package for the analysis of gas-phase chemical kinetics. Sandia National Laboratories, Livermore, CA, 1989.

[27] J. Montgomery, M.J. Frisch, J.W. Ochterski, G.A. Petersson, A Complete Basis Set Model Chemistry. VI. Use of Density Functional Geometries and Frequencies. J. Chem. Phys. 110 (1999) 2822–2827.

[28] Gaussian 09, Revision D.01, M. J. Frisch, G. W. Trucks, H. B. Schlegel, G. E. Scuseria, M. A. Robb, J. R. Cheeseman, G. Scalmani, V. Barone, B. Mennucci, G. A. Petersson, H. Nakatsuji, M. Caricato, X. Li, H. P. Hratchian, A. F. Izmaylov, J. Bloino, G. Zheng, J. L. Sonnenberg, M. Hada, M. Ehara, K. Toyota, R. Fukuda, J. Hasegawa, M. Ishida, T. Nakajima, Y. Honda, O. Kitao, H. Nakai, T. Vreven, J. A. Montgomery, Jr., J. E. Peralta, F. Ogliaro, M. Bearpark, J. J. Heyd, E. Brothers, K. N. Kudin, V. N. Staroverov, R. Kobayashi, J. Normand, K. Raghavachari, A. Rendell, J. C. Burant, S. S. Iyengar, J. Tomasi, M. Cossi, N. Rega, J. M. Millam, M. Klene, J. E. Knox, J. B. Cross, V. Bakken, C. Adamo, J. Jaramillo, R. Gomperts, R. E. Stratmann, O. Yazyev, A. J. Austin, R. Cammi, C. Pomelli, J. W. Ochterski, R. L. Martin, K. Morokuma, V. G. Zakrzewski, G. A. Voth, P. Salvador, J. J. Dannenberg, S. Dapprich, A. D. Daniels, Ö. Farkas, J. B. Foresman, J. V. Ortiz, J. Cioslowski, and D. J. Fox, Gaussian, Inc., Wallingford CT, 2009.

[29] J. Pfaendtner, X. Yu, L.J. Broadbelt, The 1-D hindered rotor approximation. Theoretical Chemistry Accounts: Theory, Computation, and Modeling. Theoretica Chimica Acta, 118 (2007) 881-898.

[30] P. Vansteenkiste, D. Van Neck,V. Van Speybroeck, M. Waroquier, An Extended Hindered-Rotor Model with Incorporation of Coriolis and Vibrational-Rotational Coupling for Calculating Partition Functions and Derived Quantities, J. Chem. Phys., 124 (2006) 044314.

[31] C. Eckart, The Penetration of a Potential Barrier by Electrons, Phys. Rev. 35 (1930) 1303.

[32] J.C. Lizardo-Huerta, B. Sirjean, R. Bounaceur, R. Fournet, Intramolecular effects on the kinetics of unimolecular reactions of β-HOROO˙ and HOQ˙-OOH radicals, Phys. Chem. Chem. Phys. 18 (2016) 12231-12251.

[33] R. Fournet, J. C.Bauge, F. Battin-Leclerc, Experimental and Modeling of Oxidation of Acetylene, Propyne, Allene and 1,3-Butadiene. Int. J. Chem. Kinet. 31 (5) (1999) 361–379.

[34] D.L. Baulch, C.J. Cobos, R.A. Cox, P. Frank, G. Hayman, T. Just, J.A. Kerr, T. Murrells, M. J. Pilling, J. Troe, R. W. Walker, J. Warnatz, Summary table of evaluated kinetic data for combustion modeling – Supplement – 1, Combust. Flame 98 (1994) 59-79.

[35] F. Battin-Leclerc, J. Biet, R. Bounaceur, G.M. Côme, R. Fournet, P-A. Glaude, X. Grandmougin, O. Herbinet, G. Scacchi, V. Warth, EXGAS-ALKANES-ESTERS: A software for the automatic generation of mechanisms for te oxidation of alkanes and esters. LRGP, UPR CNRS 3349 2010.

[36] V.V. Kislov, A.M. Mebel, J. Aguilera-Iparraguirre, W.H. Green, Reaction of Phenyl Radical with Propylene as a Possible Source of Indene and Other Polycyclic Aromatic Hydrocarbons: An Ab Initio/RRKM-ME Study. J. Phys. Chem. A, 116, (2012), 4176–4191.

[37] J. A. Manion, R. E. Huie, R. D. Levin, D. R. Burgess Jr., V. L. Orkin, W. Tsang, W. S. McGivern, J. W. Hudgens, V. D. Knyazev, D. B. Atkinson, E. Chai, A. M. Tereza, C.-Y. Lin, T. C. Allison, W. G. Mallard, F. Westley, J. T. Herron, R. F. Hampson, and D. H. Frizzell, NIST Chemical Kinetics Database, NIST Standard Reference Database 17,

Version 7.0 (Web Version), Release 1.6.8, Data version 2015.12, National Institute of Standards and Technology, Gaithersburg, Maryland, 20899-8320. Http://Kinetics.Nist.Gov/ 2016.

[38] D.-Y Peng, D. B. Robinson, A new two-constant equation of state, Ind. Eng. Chem. Fundam. 15 (1976) 59-64.

[39] J-N. Jaubert, Présentation du logiciel DiagSim permettant de faciliter l'enseignement de la thermodynamique technique, International Journal of Technologies in Higher Education 2 (2005) 34-47.

[40] V. Burklé-Vitzthum, R. Bounaceur, R. Michels, G. Scacchi, P-M. Marquaire, Kinetic parameters for the thermal cracking of simple hydrocarbons : From geological to geological time-temperature conditions, J. Anal. Appl. Pyrolysis 125 (2017) 40-49.

[41] C.H. Leigh, M.Szwarc, The pyrolysis of normal-butylbenzene and the heat of formation of normal-propyl radical, J. Chem. Phys. 20 (1952) 407-411.

[42] H. Freund, W.N. Olmstead, Detailed chemical kinetic modeling of butylbenzene pyrolysis, Int. J. Chem. Kinet. 21 (1989) 561-574.

[43] J. Yu, S. Eser, Thermal Decomposition of Jet Fuel Model Compounds under Near-Critical and Supercritical Conditions. 1. n-Butylbenzene and n-Butylcyclohexane, Ind. Eng. Chem. Res. 37 (1998)4591-4600.